

Parallel computation for natural convection

P.Wang and R.D.Ferraro

Jet Propulsion Laboratory
California Institute of Technology
MS 169-315

4800 Oak Grove Drive

Pasadena CA 91109-8099

U.S.A.

Abstract

Parallel computation for two-dimensional convective flows in cavities with adiabatic horizontal boundaries and driven by differential heating of the two vertical end walls, are investigated using the Intel Paragon, Intel Touchstone Delta, and Cray T3D. The numerical scheme, including a parallel multigrid solver, and domain decomposition techniques for parallel computing are discussed in detail. Performance comparisons are made for the different parallel systems, and numerical results using various numbers of processors are discussed.

Nomenclature

h height of cavity

l length of cavity

g acceleration due to gravity

$L = l/h$ aspect ratio of cavity

R Rayleigh number

T non-dimensional temperature

x, z non-dimensional coordinates

u, w non-dimensional velocity components

PE number of processors

Greek symbols

β coefficient of thermal expansion

ψ non-dimensional stream function

κ thermal diffusivity

ν kinematic viscosity

σ Prandtl number

ω non-dimensional vorticity function

suggest global search
for (space)(period)

1 Introduction

Convective motions driven by lateral temperature gradients in cavities are important in many areas of interest in industry and in nature. Applications include the temperature control of circuit board components under natural convection in the electronics industry, heating and ventilation control in building design and construction, cooling systems for nuclear reactors in the nuclear industry, flows and heat transfer associated with all stages of the power generation process, solar-energy collectors in the power industry and atmospheric and fluvial dispersion in the environment.

Due to the wide range of applications, studies of natural convection flow and heat transfer have been vigorously pursued for many years. A typical model of convection driven by a lateral thermal gradient consists of a two dimensional rectangular cavity with the two vertical end walls held at different constant temperatures. In order to determine the flow structure and heat transfer across cavities with different physical properties, numerous analytical, experimental and computational techniques have been used.

Experimental investigations of cavity flows driven by lateral heating have been reported in [1], [2], and [3]. In general, these flows consist of a main circulation in which fluid rises at the hot wall, sinks at the cold wall, and travels laterally across the intervening core region. The flow structure is dependent on three non-dimensional parameters: a Rayleigh number R based on the height of the cavity and the temperature difference across the end walls, the Prandtl number σ of the fluid, and the aspect ratio L (length/height).

For cavities of different aspect ratio, Rayleigh number and Prandtl number, extensive numerical results have been obtained by researchers during the past twenty-five years. Elder [4] obtained a numerical solution for a rectangular enclosure. Quon [5] carried out finite difference computations for

convection in a square cavity for a variety of dynamical boundary conditions, Rayleigh numbers and Prandtl numbers. Cormack, Leal and Seinfeld [6] obtained numerical solutions in shallow cavities for a variety of Rayleigh numbers, and more detailed numerical studies of cavity flows have been carried out in [7] and [8].

For a shallow cavity ($L \rightarrow \infty$) and Rayleigh numbers $R \ll L$ the flow is again dominated by conduction and consists of a Hadley cell driven by the constant horizontal temperature gradient set up between the end walls. Cormack, Leal and Imberger [9] predicted that the flow consists of two distinct parts: a parallel flow in the core region which extends for most of the length of the cavity and a second, non-parallel flow near the ends. Non-linear convective effects first become significant at the ends of the cavity where the flow is turned when $L = \frac{R}{2} = O(1)$. The nonlinear end-zone structure has been studied in [10], [11], and [12].

The present study focuses on parallel computation for convective flows in cavities with $L \gg 1$. The problem formulation is given in Section 2. Numerical scheme and parallel computing techniques are discussed in Section 3 and 4. The numerical results by using different parallel systems and with various numbers of processors are discussed in Section 5. Finally, conclusions are outlined in Section 6.

2 Formulation

A closed rectangular cavity of length 1 and height h is considered in which two-dimensional motions are generated by maintaining the vertical end walls at different fixed temperatures T_0 and $T_0 + \Delta T$. The cavity is filled with a fluid of kinematic viscosity ν , thermal diffusivity κ and coefficient of thermal expansion β . The appropriate governing equations, subject to the Boussinesq approximation, can

be written in dimensionless form as

$$\sigma^{-1} \left(\frac{\partial \bar{\omega}}{\partial t} + J(\bar{\omega}, \bar{\psi}) \right) = \nabla^2 \bar{\omega} + R \frac{\partial \bar{T}}{\partial x}, \quad (1)$$

$$\nabla^2 \bar{\psi} = -\bar{\omega}, \quad (2)$$

$$\frac{\partial \bar{T}}{\partial t} + J(\bar{T}, \bar{\psi}) = \nabla^2 \bar{T}, \quad (3)$$

where

$$\sigma = \frac{\nu}{\kappa} \quad (4)$$

is the Prandtl number and

$$R = \frac{g\beta\Delta T h^3}{G} \quad (5)$$

is the Rayleigh number, where g is the acceleration due to gravity. And

$$\bar{\omega} = \frac{\partial w}{\partial x} - \frac{\partial u}{\partial z} \quad (6)$$

is the vorticity, with the two Jacobians given by

$$J(\bar{\omega}, \bar{\psi}) = \frac{\partial \bar{\omega}}{\partial x} \frac{\partial \bar{\psi}}{\partial z} - \frac{\partial \bar{\omega}}{\partial z} \frac{\partial \bar{\psi}}{\partial x}, \quad J(\bar{T}, \bar{\psi}) = \frac{\partial \bar{T}}{\partial x} \frac{\partial \bar{\psi}}{\partial z} - \frac{\partial \bar{T}}{\partial z} \frac{\partial \bar{\psi}}{\partial x}. \quad (7)$$

The boundary conditions on the cavity walls are

$$\bar{\psi} = \frac{\partial \bar{\psi}}{\partial x} = 0, \quad x = 0, L; \quad \bar{\psi} = \frac{\partial \bar{\psi}}{\partial z} = 0, \quad z = 0, 1 \quad (8)$$

$$\bar{T} = 0, \quad x = 0; \quad \bar{T} = 1, \quad x = L \quad (9)$$

with

$$\frac{\partial \bar{T}}{\partial z} = 0 \quad \text{on } z = 0, 1 \quad (10)$$

for insulated walls, where

$$L = \frac{l}{h} \quad (11)$$

is the aspect, ratio of the cavity.

It is easily verified that the governing equations and boundary conditions are consistent with Gill's [13] centro-symmetry relations

$$\begin{aligned}\bar{\psi}(x, z, t) &= \bar{\psi}(L - x, 1 - z, t), \\ \bar{T}(x, z, t) &= 1 - \bar{T}(L - x, 1 - z, t) \\ \bar{\omega}(x, z, t) &= \bar{\omega}(L - x, 1 - z, t)\end{aligned}\quad (12)$$

which, for appropriate initial conditions, effectively allow only one half of the flow domain to be considered,

The formal asymptotic structure of the steady flow in a shallow cavity where $L \gg 1$ and $R_1 = R/L = O(1)$ is studied by Daniels et al [11]. Further details about core solution, end-zone problem, and numerical study in shallow cavities are discussed in [14]. Throughout most of the cavity (the core region) the flow is dominated by the lateral conduction associated with a Hadley circulation, so that

$$\bar{T} = \xi + L^{-1} \left\{ \left(\xi - \frac{1}{2} \right) c_1(R_1, \sigma) + R_1 F(z) \right\} + O(L^{-2}) \quad (13)$$

and

$$\bar{\psi} = R_1 \{ 1 + L^{-1} c_1(R_1, \sigma) \} F'(z) + O(L^{-2}) \quad (14)$$

as $L \rightarrow \infty$, where $\xi = \frac{x}{L}$,

$$F(z) = \frac{z^5}{120} - \frac{1}{48} z^4 + \frac{1}{72} z^3 - \frac{1}{1440} \quad (15)$$

and $c_1(R_1, \sigma)$ is a constant contribution determined by matching with solutions near the end wall.

Near the cold wall, the solution adjusts to the boundary conditions (8)-(10) in a square zone where $x, z = O(1)$,

$$\bar{T} = L^{-1} T(x, z, t) + \dots, \bar{\psi} = \psi(x, z, t) + \dots, \bar{\omega} = \omega(x, z, t) + \dots \quad (L \rightarrow \infty)$$

Okay, a space after the equation before a comma or a period. But if you do it, it should be consistent.

and substitution into (1)-(3) indicates that a steady-state solution of the system

$$\sigma^{-1} \left(\frac{\partial \omega}{\partial t} + J(\omega, \psi) \right) = \nabla^2 \omega - R_1 \frac{\partial T}{\partial x}, \quad (16)$$

$$\nabla^2 \psi = -\omega, \quad (17)$$

$$\frac{\partial T}{\partial t} + J(T, \psi) = \nabla^2 T, \quad (18)$$

is required. From (8-11) these equations are to be solved subject to

$$\psi = \frac{\partial \psi}{\partial z} = \frac{\partial T}{\partial z} = 0 \quad \text{on} \quad z = 0, 1, \quad (19)$$

$$\psi = \frac{\partial \psi}{\partial x} = T = 0 \quad \text{on} \quad x = 0, \quad (20)$$

and to match with the core solution

$$\psi \rightarrow R_1 F'(z), \quad T \sim x + c + R_1 F(z) \quad (x \rightarrow \infty) \quad (21)$$

The core temperature is determined to order L^{-1} through the matching requirement

$$c_1 = -2C \quad (22)$$

but the value of c itself can only be determined by solving the end-zone problem (16)-(22). The aim of the present work is to determine such solutions (1)-(11) *on* the whole flow domain or (16)-(22) on the end-zone region if $L \gg 1$ and $R_1 = R/L = O(1)$ numerically by an effective parallel solver.

3 Numerical Scheme for the Systems

In order to solve the system (16)-(22) numerically, a finite difference method is considered. It was decided to employ an explicit method based on the Dufort-Frankel scheme outlined in [15] to follow the evolution of the system, in preference to an implicit method. Methods of the latter type (for

example Crank and Nicholson, Peaceman and Rachford) have the advantage of unconditional numerical stability, allowing a large time step to be used, but involve the solution of large matrix systems at each time step. Like these methods, the Dufort-Frankel method has second order accuracy and although it must meet a Courant condition to maintain numerical stability, it involves significantly less computational time at each time step.

The heat equation (18) is discretized using central differences in x and z and Arakawa's scheme [16] for the Jacobian term, to be denoted here by J , leading to an explicit expression for the temperature $T_{i,j}^{k+1}$ at internal grid points of the form

$$T_{i,j}^{k+1} = \frac{\frac{\Delta t(T_{i+1,j}^k + T_{i-1,j}^k)}{(\Delta x)^2} + \frac{\Delta t(T_{i,j+1}^k + T_{i,j-1}^k)}{(\Delta z)^2} - \Delta t J(T_{i,j}^k, \psi_{i,j}^k) + x_1 T_{i,j}^{k-1}}{x_2}, \quad (23)$$

where

$$x_1 = \frac{1}{2} \frac{\Delta t}{(\Delta x)^2} \cdot \frac{\Delta t}{(\Delta z)^2},$$

$$x_2 = \frac{1}{2} \frac{\Delta t}{(\Delta x)^2} + \frac{\Delta t}{(\Delta z)^2}$$

At the lower horizontal boundary the temperature can be found using the second order formula

$$T_{i,0}^{k+1} = \frac{\frac{\Delta t}{(\Delta x)^2} [T_{i+1,0}^k + T_{i-1,0}^k] + \frac{\Delta t}{(\Delta z)^2} 2T_{i,1}^k + x_1 T_{i,0}^{k-1}}{x_2}, \quad (24)$$

obtained using the boundary condition $\partial T / \partial z = 0$ while a similar formula is applicable at the upper boundary. At the cold wall $T_{0,j}^{k+1} = 0$, while the boundary condition on the hot wall takes $T_{N,j}^{k+1} = 1$.

The vorticity equation (16) is treated in a similar manner, and at internal grid points

$$\omega_{i,j}^{k+1} = \frac{\frac{\Delta t}{(\Delta x)^2} (\omega_{i+1,j}^k + \omega_{i-1,j}^k) + \frac{\Delta t}{(\Delta z)^2} (\omega_{i,j+1}^k + \omega_{i,j-1}^k) - \Delta t \sigma^{-1} J(\omega_{i,j}^k, \psi_{i,j}^k)}{\bar{x}_2},$$

$$+ \frac{\frac{\Delta t}{2\Delta x} R(T_{i+1,j}^k - T_{i-1,j}^k) + \bar{x}_1 \omega_{i,j}^{k-1}}{\bar{x}_2} \quad (25)$$

where

$$\bar{x}_1 = \frac{1}{2\sigma} - \frac{\Delta t}{(\Delta x)^2} - \frac{\Delta t}{(\Delta z)^2},$$

$$\bar{x}_2 = \frac{1}{2\sigma} + \frac{\Delta t}{(\Delta x)^2} + \frac{\Delta t}{(\Delta z)^2}$$

with the Jacobian term discretized using Arakawa's scheme. The vorticity at the cold wall can be determined in the second-order accurate form

$$\omega_{0,j} = \frac{1}{2(\Delta x)^2} (8\psi_{2,j} - \psi_{1,j}), \quad j = 0, 1, 2, \dots, N_z. \quad (26)$$

Similar formulae are used for the upper, lower, and the right boundaries.

The explicit formulae (23-24) and (25) constitute a three-layer scheme and so an alternative method is needed on the first time step to initiate the computation. Here an iterative scheme based on Successive Over-Relaxation (SOR) was used to solve the equations discretized as a second-order accurate implicit system and further details this are given in [12].

A five-point multigrid method is used to solve the Poisson equation (17) for the stream function at each time step, with the solution for a coarse grid used to revise the required solution on a fine grid. The central difference approximation of equation at internal grid points is written in the form

$$\psi_{i,j} = \frac{(\Delta z)^2(\psi_{i+1,j} + \psi_{i-1,j}) + (\Delta x)^2(\psi_{i,j+1} + \psi_{i,j-1}) + \omega_{i,j}(\Delta x)^2(\Delta z)^2}{2(\Delta x)^2 + 2(\Delta z)^2} \quad (27)$$

and then Successive Over-Relaxation used to obtain the solution within the multigrid scheme, which is described in full in [17]. On the all boundaries, ψ is zero. At the present study, a parallel 4-level-grid Poisson solver has been implemented on different parallel systems, based on the domain

decomposition technique. A V-Cycle scheme is considered in this code with the SOR method as a smoother. More details about parallel implementations will be given in the next section.

The overall scheme of computation for a given Rayleigh number, Prandtl number and Aspect ratio can be described as follows. An initial state was usually taken either in the form of a conductive solution with no motion $\psi = 0$, $\omega = 0$ ($0 \leq x \leq L$) or in the form of a steady-state solution obtained at a lower Rayleigh number R . The temperature, vorticity and stream function fields are then found in succession at each time step, using the modified scheme for subsequent time steps. The computation continues until a steady-state solution is achieved, as measured by the maximum differences between successive values of T and ω .

4 Parallel Computing Techniques

4.1 Computing Systems

A parallel computing system may be thought of as a collection of n computers which communicate with each other over some kind of communications network. A system with thousands of processors is called massively parallel, and holds the greatest promise for significantly extending the range of practically solvable computational problems. A diametrically opposite option is coarse-grained parallelism, in which there is a small number of processors. In this case, each processor is usually fairly powerful, and the processors are loosely coupled, so that each processor may be performing a different type of task at any given time. A significant aspect of parallel computers is the mechanism by which processors exchange information. Generally speaking, there are two types, known as shared memory and message-passing architectures. The first uses a global shared memory that can be accessed by all processors, and in the second case, there is no shared memory, but rather each

processor has its own local memory. **Processors** communicate through an interconnection network consisting of direct communication links joining **certain** pairs of processors. Some systems might have a shared memory, and at the same time each processor has its own local memory. In the following, three different parallel systems will be introduced, which are the major computing systems for the present work.

Intel Touchstone Delta: The Delta at the Concurrent Supercomputing Consortium at California Institute of Technology is a message-passing **MIMD (Multiple Instruction Multiple Data) multicomputer**, consisting of an ensemble of individual and autonomous nodes that communicate across a **two-dimensional** mesh interconnection network. It has 512 computational **i860** nodes, each with 16 M bytes of memory and each node has a peak speed of 60 **MegaFLOPS**. A Concurrent File System (CFS) is attached to the nodes with a total of 95 Gbytes of formatted disk space. The operating system is **Intel's Node Executive** for the mesh (N X/M).

IntelParagon XI/S: This MIMD distributed machine has a 2D mesh topology, with a faster processor and network speed than the Delta system. The one at the Jet Propulsion Laboratory is currently configured with 56 compute nodes, and each one has a peak speed of 75 **MegaFLOPS** and 32 **Megabytes** memory. The operating system is the Paragon **OSF/1**, based on the **OSF/1** operating system from the Open Software Foundation. The NX communication library was used for the present study, which makes it portable to the Delta machine.

Cray T3D: The Cray T3D at JPL, currently one of the most powerful MIMD computers available, has 256 compute nodes with 150 **MegaFLOPS** peak performance and 64 **Megabytes** memory per node. Logically, it has a shared memory, and physically a distributed memory, associated with a processor. It uses a three-dimensional Torus as the interconnect network. A message passing

library is available, based on **PVM3** software developed by the Oak Ridge National Laboratory, the University of Tennessee, and Emory University. Numerical results from these systems will be discussed later.

4.2 Domain Decomposition

In order to implement a parallel code with the **Dufort-Frankel-Multigrid** method for natural convective flow problems in rectangular cavities, a **two-dimensional** original fine mesh is partitioned into blocks of consecutive columns ($L \gg 1$) and distributed onto a logically linear array of processors (Figure 1). Each processor has a **subdomain** (Figure 2), and the whole computational job is divided into n subjobs if n processors are used. This is a natural way for data partitioning with the above geometries since the communication among subdomains needs to be minimized. Once the partition structure is set up, the next concern is about how to update all information at neighbors in each subdomain to keep the computation continuous over the whole computational domain.

4.3 Parallel Dufort-Frankel-Multigrid Algorithms

One of the major concerns in the design of a parallel code is communications. The major part of communication is that each subdomain needs to exchange information with its neighbors and this is done by **direct** message-passing software at each iterative level on Intel Paragon, Delta, and Cray T3E. Since only the values at the boundaries of each subdomain need to be updated at each iteration, the **total** amount of communication is still relatively small comparing with the whole computation. The other part of communication occurs in I/O operations. The main structure of the parallel algorithm for the whole computation is briefly summarized by the following steps:

1. Partition the computational mesh.

2. *Set* initial conditions on each subdomain.
3. Exchange edge values with neighboring processors.
4. Perform Dufort-Frankel update $T_{i,j}^{(k)}$ locally on each processor.
5. Perform Dufort-Frankel update $\omega_{i,j}^{(k)}$ locally at all interior grid points on each processor,
6. Perform parallel Multigrid update of $\psi_{i,j}^{(k)}$ on all processors
7. Perform boundary calculations for $\omega_{i,j}^{(k)}$ on all processors involving boundaries.
8. Check conditions for a steady-state solution. If satisfied, stop. Otherwise,
advance time step $k \leftarrow k + 1$, and go to 3.

And the parallel Multigrid solver is summarized as the following:

For the Poisson equation $\nabla^2 \psi = -w$, the discrete form can be written as $A\psi^h = \omega^h$, and the parallel V-Cycle scheme $\psi^h \leftarrow M\psi^h(\psi^h, \omega^h)$ with total grid levels $= N$ is outlined as :

1. Do $k = 1, N - 1$

Relax n_1 times on $A^h \psi^h = \omega^h$ with a given initial guess ψ^h , and after each relaxation iteration, exchange edge values with neighbors.

$$w^{2h} \leftarrow J_h^{2h}(\omega^h - A^h \psi^h), \quad \psi^{2h} \leftarrow 0$$

Enddo

2. $k = N$ (the coarsest grid), solve $A^h \psi^h = \omega^h$

3. Do $k = N - 1, 1$

$$\text{Correct } \psi^h \leftarrow \psi^h + J_{2h}^h \psi^{2h}.$$

Relax n_2 times on $A^h \psi^h = \omega^h$ with initial guess ψ^h , and after each relaxation iteration, exchange edge values with neighbors.

Enddo

Here I_h^{2h} and I_{2h}^h are restriction operator and interpolation operator respectively, and in the present study, injection and linear interpolation are used. An example of Multigrid structures with a partitioning on 4 processors is given in Figure 3. The data distribution on each processor on one grid level is illustrated in Figure 4, and a similar strategy is used for the rest of the grid levels. Here each processor needs to store its own subdomain data and its neighbor boundary data as well.

5 Results and Discussion

Various numerical experiments have been carried out on the Intel Delta, the Intel Paragon, and Cray T3D. A model with $R_1 = 200$, $\sigma = 0.733$, $L = 16$, and mesh $= 64 \times 1024$ was tested on those machines. The computation is stopped when the following conditions are satisfied, corresponding to the attainment of a steady-state solution:

$$\max_{i,j} |T_{i,j}^{k+1} - T_{i,j}^k| < \epsilon_1,$$

$$\max_{i,j} |\omega_{i,j}^{k+1} - \omega_{i,j}^k| < \epsilon_2,$$

where k is the time level index and ϵ_1 and ϵ_2 are usually taken to be 10^{-6} .

In order to compare the performance on each system, 16 processors were used for the parallel code with the above numerical model. The computation results are showed in Table 1, which lists the total CPU time on the test problem for the three systems. The Cray T3D gives the best performance, and the Paragon shows better performance than the Delta. By various tests on the parallel systems and comparisons with some previous results, the parallel code is proven numerically stable, efficient, and reliable.

Numerical results were obtained for various Rayleigh numbers and Prandtl numbers. Here results for the flow in water are discussed. The solution for $R_1 = 2000$ and $\sigma = 6.983$ in the steady-state

are illustrated in Figure 5 by the contour plots of stream function, vorticity, and temperature. The results have been compared with the asymptotic structures predicted by boundary-layer theory [18]. According to asymptotic predictions, for $\sigma = 0.733$ $c_0 = 5.2849 \times 10^{-5}$, the c in (21) satisfies $c \sim R_1^{7/5} c_0$ (a). Our numerical computation gives $c_0 = 4.9605 \times 10^{-5}$ which is in excellent agreement with the theoretical prediction. Since the theory is based on high Rayleigh number, numerical simulation for higher Rayleigh number in the case of water will be considered in future work.

For low Prandtl numbers with a small aspect ratio, numerical computation for the whole cavity is considered. Figure 6 shows the contour plots of stream function, vorticity, and temperature for $\sigma = 0.005$, $R = 400$, and $L = 4$ with a mesh size equal to 64×1024 . The results show the existence of secondary flow consistent with linear stability analysis in [10] and [11].

More numerical experiments have been investigated on the Cray T3D with various numbers of processors. Figures 7 and 8 are the scaling performances of the parallel computation code. Various meshes have been used with a test model of $RI = 400$, $\sigma = 0.733$, $L = 64$ for a fixed time steps. The largest problem has a global grid of 256×32768 distributed on 256 processors, with total unknowns of 41,744, 384. Figure 7 shows the ratio of execution time $T(1)/T(n)$ versus the number of processors. $T(1)$ is the execution time of a code for a given problem on one processor and $T(n)$ is the execution time of a code for a given problem on n processors. Figure 8 shows the scaling performance for large global grids on the Cray T3D. These figures show that the speed up from 1 processor to 256 processors goes well for a larger grid, but for a small problem, it starts to slow down when more processors come to play. This is mainly due to the computational load for a small problem is relatively small and the communication part weights much heavier for the whole code when a large number of processors is used. it will be no longer the best strategy to partition the

computational domain into blocks of columns if the number of processors is much larger than the aspect ratio L of a cavity. In this case, 2D partitioning should be applied, which will be considered in our future work. More numerical results for high Rayleigh numbers and large grids on parallel systems are given in the forthcoming paper [19].

6 Conclusions

In this paper, a detailed numerical study of natural convection has been described with different parallel systems. A domain decomposition technique has been efficiently used in solving the Poisson equation with a Multigrid method and the other two time-dependent equations with the Dufort-Frankel scheme. The parallel code shows good convergence and efficiency which indicate the potential of parallel systems for solving large complicated fluid dynamics problems. The present numerical solutions appear to be in good agreement with theoretical predictions. The discrepancy of CPU for the whole computation on the three systems is due to the difference of hardware on each system and the network connection used. Obviously, from the point view of speed, the Cray T3D ranks first, and the Paragon is slightly faster than the Delta.

7 Acknowledgments

The research described in this paper was carried out by the Jet Propulsion Laboratory, California Institute of Technology, and was sponsored by the National Research Council and the National Aeronautics and Space Administration while one of the authors (P. Wang) held a NRC-JPL Research Associateship.

Reference herein to any specific commercial product, process, or service by trade name, trade-

mark, manufacturer, or otherwise, does not constitute or imply its endorsement by the United States Government, the National Research Council, or the Jet Propulsion Laboratory, California Institute of Technology.

This research was performed in part using the CSCC parallel computer system operated by Caltech on behalf of the Concurrent Supercomputing Consortium. Access to this facility was provided by NASA.


The Cray Supercomputer used in this investigation was provided by funding from the NASA Offices of Mission to Planet Earth, Aeronautics, and Space Science.

Access to the Intel Paragon at the Jet Propulsion Laboratory, California Institute of Technology, was provided by the NASA High Performance Computing and Communications Office.

References

- [1] J. Imberger. Natural convection in a shallow cavity with differentially heated end walls. Part 3. Experimental results. *Journal of Fluid Mechanics*, 65:247-260, 1974.
- [2] P.G. Simpkins and K.S. Chen. Convection in horizontal cavities. *Journal of Fluid Mechanics*, 166:21-39, 1986.
- [3] J. C. Patterson and S. W. Armfield. Transient features of natural convection in a cavity. *Journal of Fluid Mechanics*, 219:469-497, 1990.
- [4] J.W. Elder. Numerical experiments with free convection in a vertical slot. *Journal of Fluid Mechanics*, 24:823-843, 1966.

- [5] C. Quon. High Rayleigh number convection in an enclosure- a numerical study. *Physics of Fluids*, 15:12-19, 1972.
- [6] D. It. Cormack, L. G. Leal, and J. H. Seinfeld. Natural convection in a shallow cavity with differentially heated end walls. Part 2. Numerical solutions. *Journal of Fluid Mechanics*, 65:231-246, 1974.
- [7] A. Bejan and C. I. Tien. Laminar natural convection heat transfer in a horizontal cavity with different end temperatures. *Trans. A.S.M.E.: Journal of Heat Transfer*, 100:641-647, 1978.
- [8] J. E. Drummond and S. A. Korpela. Natural convection in a shallow cavity. *Journal of Fluid Mechanics*, 182:543-564, 1987,
- [9] D. It. Cormack, L. G. Leal, and J. Imberger. Natural convection in a shallow cavity with differentially heated end walls, Part 1. Asymptotic theory. *Journal of Fluid Mechanics*, 65:209-229, 1974.
- [10] J. E. Hart. Low Prandtl number convection between differentially heated end walls. *International Journal of Heat and Mass Transfer*, 26:1069-1074, 1983.
- [11] P. G. Daniels, P. A. Blythe, and P. G. Simpkins. Onset of multicellular convection in a shallow laterally heated cavity. *Proceeding of Royal Society, A*, 411:327-350, 1987.
- [12] P. Wang. *Thermal Convection in Slender Laterally-Heated Cavities*. Ph.D. Dissertation, City University, London, 1992.
- [13] A. E. Gill. The boundary-layer regime for convection in a rectangular cavity. *Journal of Fluid Mechanics*, 26:515-536, 1966.

- 
- [14] P. Wang and P. G. Daniels. Numerical solutions of the flow near the end of a shallow laterally heated cavity. *Journal of Engineering Mathematics*, 28:211-226, 1994.
- [15] P.J.Roache. *Computational Fluid Dynamics*. Hermosa,Alberquerque,N. Mex., 1976
- [16] A. Arakawa. Computational design for long-term numerical integration of the equations of fluid motion: Two dimensional incompressible flow, part 1. *Journal of Computational Physics*, 1:119-143, 1966.
- [17] A. Brandt. Multi-level adaptive solutions to boundary-value problems. *Mathematics of Computation*, 31:333--390, 1977.
- [18] P.G.Daniels.High Rayleigh number thermal convection in a shallow laterally heated cavity. *Proceeding of Royal Society, A*, 440:273-289, 1993.
- [19] P. Wang and R.D.Ferraro. A numerical study of high Rayleigh number thermal convection in shallow cavities. *Journal of Fluid Mechanics*, Submitted, 1995.

- Just got your info
table is a bit confusing
- Do the parameters apply to all systems?
If so, they could be in the text or caption.
 - If 16 processors is for all, it should be ahead of the computer names, otherwise, it sounds like just the Cray has 16 processors

bad once better
for headings

Parameters	system	CPU	Time (s)
$Mesh = 64 \times 1024$	Intel Touchstone Delta	1099	
$R = 10^4, u = 0.733$	Intel Paragon	824	
$L = 16$	Cray T3D	197	

Table CPU times (seconds) for the Delta, the Paragon, and the Cray T3D using 16 processors.

List of Figures

1. An example of Computational mesh 4×16 with 4 processors.
2. Data partition on the computational domain
3. Data partition of 4×16 fine grid and the derived coarse grids with 4 processors.
4. Data distribution on each processors for 4×16 grid.
5. Contoursof the steady-state solution for (a) stream function, (b) vorticity, (c) temperature, for $\sigma = 6.983$, $R_1 = 2 \times 10^3$, and $x_\infty = 16$, using a 64×1024 computational rid.
6. Contour plots for (a) stream function, (b) vorticity, (c) temperature, for $\sigma = 0.005$, $R = 4 \times 10^4$, and $L = 4$, using a 64×1024 computational grid for the whole cavity.
7. Speed up of the parallel code on the Cray T3D
8. Scaling performance on the Cray T3D

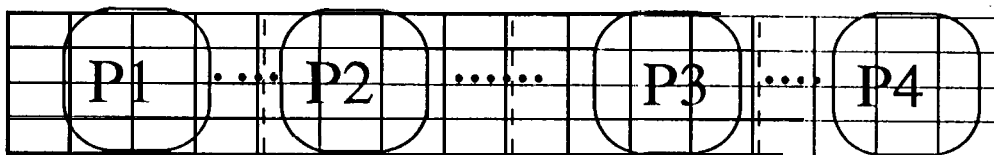


Fig. 1

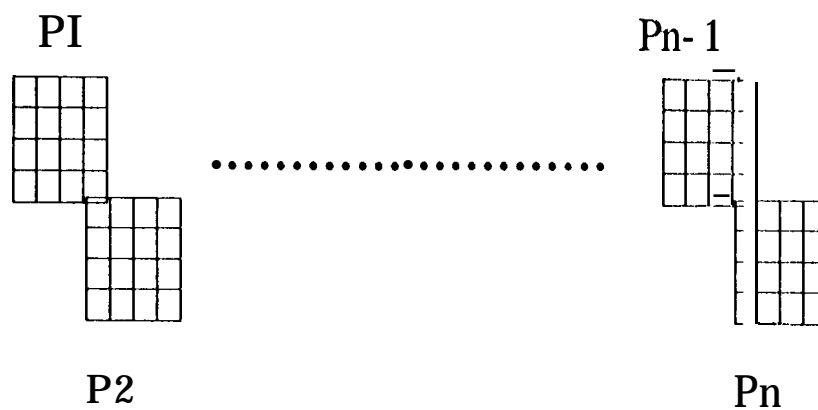
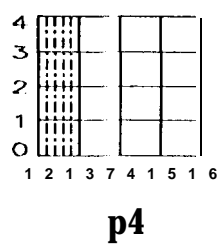
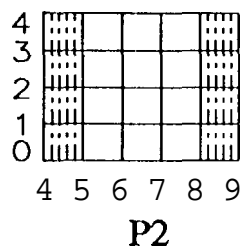
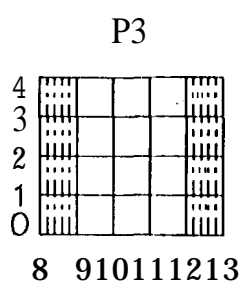
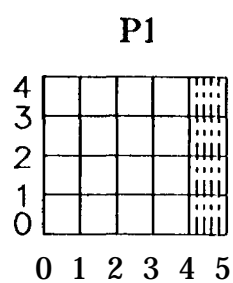


Fig. 2



--	--	--	--

P1

P2

P3

P4

P1

P2

P3

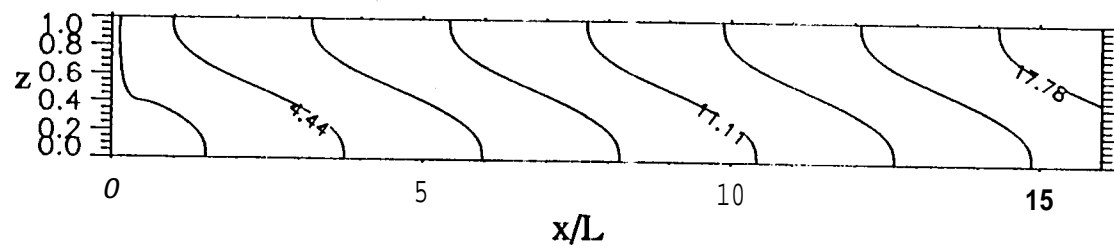
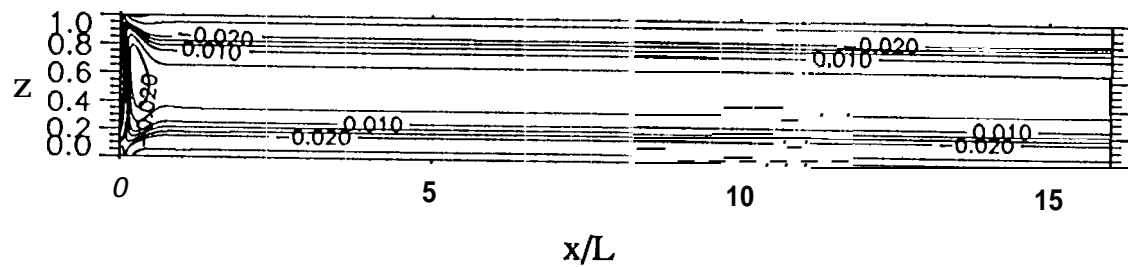
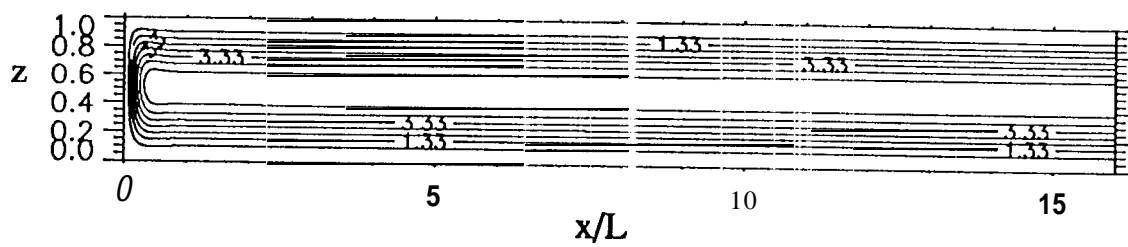
P4

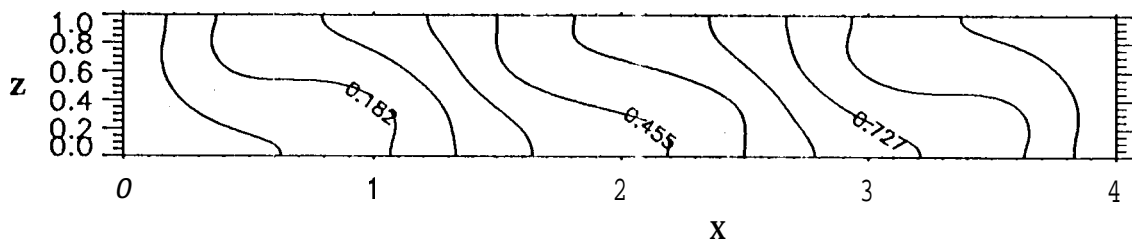
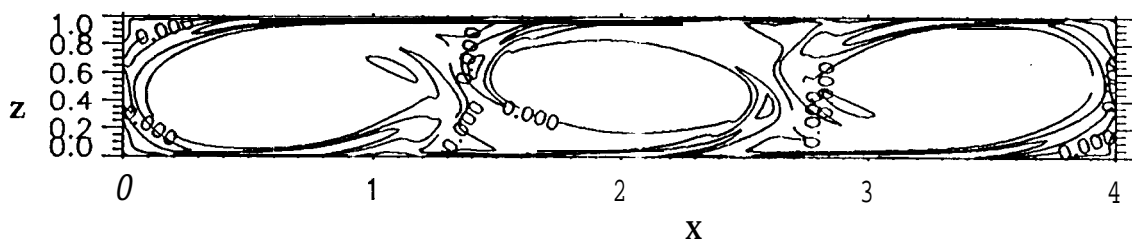
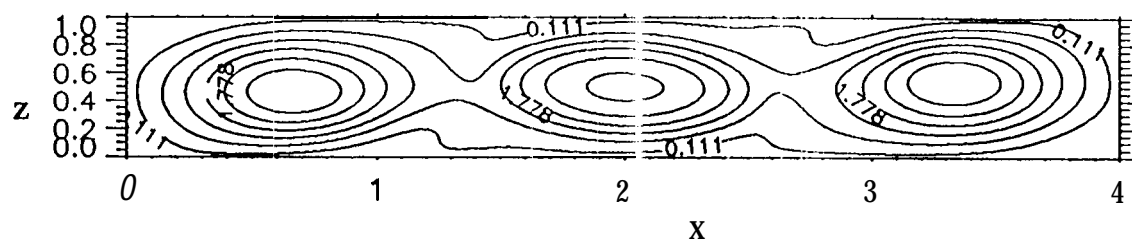
P1

P2

P3

P4





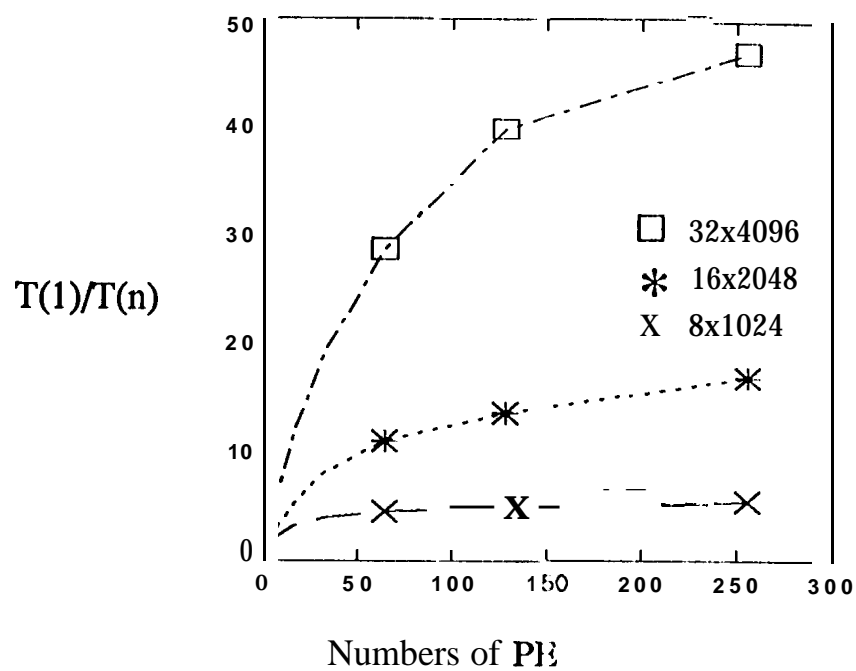


Fig. 7

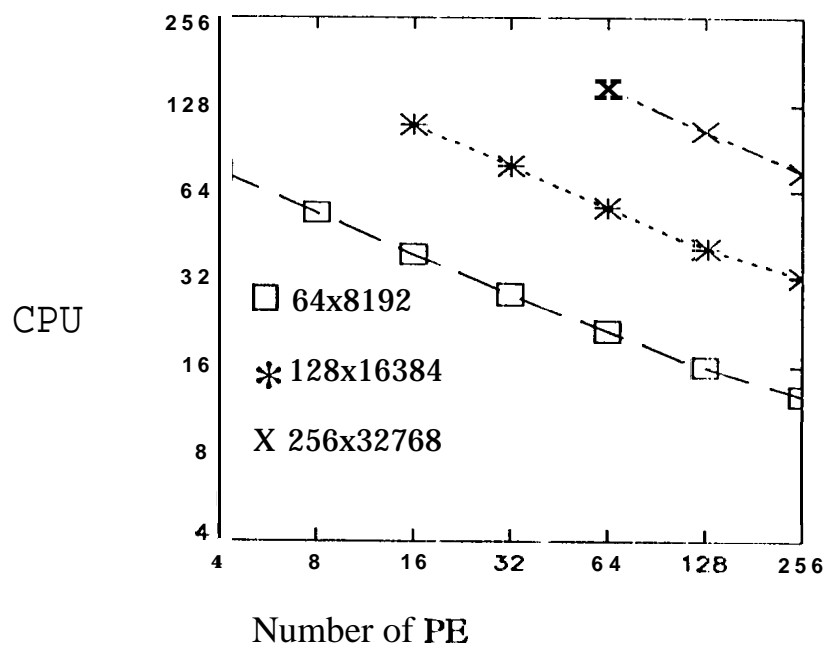


Fig. 8